

Journal Pre-proof

Effect of noble metal element on microstructure and NO₂ sensing properties of WO₃ nanoplates prepared from a low-grade scheelite concentrate

Tingting Li, Yanbai Shen, Xiangxi Zhong, Sikai Zhao, Guodong Li, Baoyu Cui, Dezhou Wei, Kefeng Wei

PII: S0925-8388(19)34173-8

DOI: <https://doi.org/10.1016/j.jallcom.2019.152927>

Reference: JALCOM 152927

To appear in: *Journal of Alloys and Compounds*

Received Date: 23 July 2019

Revised Date: 4 November 2019

Accepted Date: 5 November 2019

Please cite this article as: T. Li, Y. Shen, X. Zhong, S. Zhao, G. Li, B. Cui, D. Wei, K. Wei, Effect of noble metal element on microstructure and NO₂ sensing properties of WO₃ nanoplates prepared from a low-grade scheelite concentrate, *Journal of Alloys and Compounds* (2019), doi: <https://doi.org/10.1016/j.jallcom.2019.152927>.

This is a PDF file of an article that has undergone enhancements after acceptance, such as the addition of a cover page and metadata, and formatting for readability, but it is not yet the definitive version of record. This version will undergo additional copyediting, typesetting and review before it is published in its final form, but we are providing this version to give early visibility of the article. Please note that, during the production process, errors may be discovered which could affect the content, and all legal disclaimers that apply to the journal pertain.

© 2019 Published by Elsevier B.V.



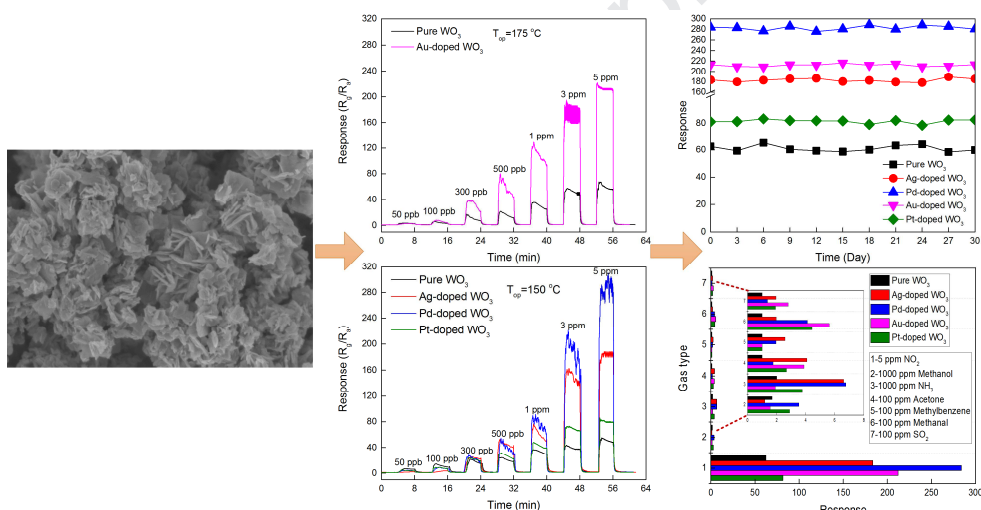
Effect of noble metal element on microstructure and NO₂ sensing properties of WO₃ nanoplates prepared from a low-grade scheelite concentrate

Tingting Li ^a, Yanbai Shen ^{a,*}, Xiangxi Zhong ^a, Sikai Zhao ^a, Guodong Li ^a,
Baoyu Cui ^{a,*}, Dezhou Wei ^a, Kefeng Wei ^b

^a School of Resources and Civil Engineering, Northeastern University, Shenyang 110819, China

^b Shen Kan Engineering and Technology Corporation, MCC., Shenyang, 110169, China

E-mail: shenyanbai@mail.neu.edu.cn; Tel/Fax: +86-24-83687381.cuibaoYu@mail.neu.edu.cn.



The noble metal-doped WO₃ nanoplates were synthesized from a low-grade scheelite concentrate for NO₂ detection with enhanced sensing performances.

Effect of noble metal element on microstructure and NO₂ sensing properties of WO₃ nanoplates prepared from a low-grade scheelite concentrate

Tingting Li ^a, Yanbai Shen ^{a,*}, Xiangxi Zhong ^a, Sikai Zhao ^a, Guodong Li ^a,

Baoyu Cui ^{a,*}, Dezhou Wei ^a, Kefeng Wei ^b

^a School of Resources and Civil Engineering, Northeastern University, Shenyang 110819, China

^b Shen Kan Engineering and Technology Corporation, MCC., Shenyang, 110169, China

*Corresponding author. Tel. & Fax: +86-24-8368-7381.

E-mail: shenyanbai@mail.neu.edu.cn (Y. Shen). cuibaoyu@mail.neu.edu.cn (B. Cui)

ABSTRACT

To break the limitation of raw materials for preparing functional WO₃ nanomaterials, a low-grade scheelite concentrate was selected as the tungsten source, and WO₃ nanoplates doped with Ag, Pd, Au and Pt were synthesized through three combined processes including NaOH leaching, chemical precipitation and acidification. The microstructure and NO₂ sensing properties of pure and noble metal-doped WO₃ nanoplates were investigated. The microstructure characterization demonstrated that all WO₃ products were composed of interlaced and irregular nanoplates with the thickness of 10–30 nm, and the length and width of these nanoplates were in the range of several hundred nanometers. NO₂ sensing properties indicated that WO₃ nanoplates doped with noble metal nanoparticles exhibited obviously higher responses and shorter response times than pure WO₃ nanoplates. Especially, noble metal-doped WO₃ nanoplates exhibited distinct behaviors in terms of the enhancement of sensing properties. Pd-doped WO₃ nanoplates exhibited highest response to NO₂, and Ag-doped WO₃ nanoplates exhibited fastest response speed. Additionally, Ag-, Pd- and Pt-doped WO₃ nanoplates exhibited a relatively lower optimal operating temperature. The enhanced NO₂ sensing performance can be ascribed to the large specific surface area of WO₃ nanoplates, the catalytic activities of noble metal nanoparticles, and the varied work function energies together with the lower activation energies.

Keywords: Scheelite concentrate; Noble metal doping; WO₃ nanoplates; NO₂; Gas sensing mechanism

1. Introduction

Over the past few decades, air pollution has attracted more and more attention due to its serious harm to environment and human health. Therefore, there is an increasing requirement for the detection of toxic and explosive gases like NO_x , H_2S , H_2 , SO_2 , NH_3 and so on [1, 2]. Among these detrimental gases, NO_2 is a sort of corrosive and poisonous gas, which is mainly derived from the exhaust of industrial plants and automobile engines as well as high-temperature combustion of fossil fuels [3-6]. It is a main contributor to acid rain and also can bring about a variety of adversely environmental effects such as visibility reduction, ozone layer thinning and acidification [7-9]. More importantly, NO_2 is extremely harmful to human health, which can damage human's respiratory system at a relatively low concentration [10]. Therefore, numerous efforts have been made to develop NO_2 sensor for detecting low-concentration even ppb-level NO_2 .

Recently, semiconductor metal oxides (SMO), such as WO_3 , ZnO , In_2O_3 , NiO and SnO_2 have received considerable attention in the field of gas sensors such as atmosphere detection, medical diagnosis, automobile emission inspection, fossil fuel combustion control, food processing, and homeland security due to their obvious advantages such as low cost, high response, simple implementation, outstanding selectivity, and compatibility with micro-assembly technology [11-18]. Especially among the numerous gas sensing materials, tungsten oxide (WO_x) with a wide band gap from 2.4 to 2.8 eV, an important n-type functional semiconductor material, has attracted more and more attention due to its outstanding sensing performance such as

high sensitivity, good stability, fast response/recovery speed, and extraordinary selectivity towards various gases, specially towards NO_2 [3, 8, 19-22]. Over the past few years, for the sake of meeting the needs of practical application, considerable efforts have been devoted to improve gas sensing properties. As a consequence, various nanoscale WO_3 nanomaterials, including nanoplates [23, 24], nanoparticles [25], nanotubes [26], nanorods [27], nanofibers [28], and nanospheres [29] have been successfully prepared and showed enhanced sensing properties for different detected gases. However, as far as we know, the raw materials for preparing functional WO_3 nanomaterials are mainly analytical pure reagents such as sodium tungstate, ammonium metatungstate and tungsten hexachloride, or tungsten metal. These chemicals are relatively expensive and complex in preparation process, which extremely restricts their large-scale application and inevitably brings about some environmental pollution in their preparation processes. Therefore, using a cheaper tungsten-containing raw material to synthesize WO_3 nanomaterials will provide a new idea for the development of functional tungsten nanomaterials. To the best of our knowledge, there are few reports on the synthesis of functional WO_3 nanomaterials by using some tungsten-containing raw materials. Hence, it is believed that this will be an interesting insight in material science, which will be an efficient and cost-effective method to prepare functional nanomaterials.

Additionally, a variety of noble metal elements may exist in tungsten ores, which are beneficial to the improvement of the gas sensing performance of functional WO_3 nanomaterials. As is well known, some noble metal elements (Pd, Ag, Pt and Au) can

be used to enhance the sensing performance of WO_3 nanomaterials due to their sensitization effects together with thermally and chemically stable for long-term operation [30, 31]. Some studies demonstrated that the enhanced sensing properties could be ascribed to the reduced activation energy of the chemical reactions between sensing material and the detected gas due to noble metal's catalytic effect, so that it could more easily react with detected gases [32, 33]. Several works have been carried out to identify the sensitization role of noble metal dopants. For instance, Akbar et al. [34] reported that the addition of noble metal had a wide influence on catalytic activity, gas adsorption, and band bending of semiconducting oxide nanomaterials. Kamble et al. [35] prepared Ag-decorated WO_3 gas sensor, which exhibited an obviously enhanced NO_2 sensing performance compared with pure one and could be used for the detection of sub-ppm level NO_2 concentration. Wu et al. [36] prepared the Pd-doped mesoporous WO_3 sensor, which had a higher response to H_2 in comparison with pure one. Zhang et al. [7] synthesized bilayer Au nanoparticle-decorated WO_3 porous thin films, revealing that Au doping could not only improve NO_2 sensing performance but also reduce the optimal operating temperature as well as the response/recovery speed. Gu et al. [31] studied the atomically dispersed Pt(II) on WO_3 for catalytic oxidation and highly selective sensing of trimethylamine. They indicated that the atomically dispersed Pt(II) on WO_3 not only decreased the activation energy, but also increased the number of active sites, which resulted in an enhancement in the gas sensing properties. These studies mainly focused on the effect of a single noble metal on WO_3 sensing materials. However, there are few reports

related to the modification of nanostructured WO_3 sensing materials with different noble metal elements.

Herein, a low-grade scheelite concentrate was selected as the tungsten source, where the sodium tungstate-containing leaching solution was firstly obtained by a high-pressure leaching method with sodium hydroxide as the leaching agent. Then calcium tungstate was prepared by a chemical precipitation method. Subsequently, using the as-obtained calcium tungstate as the precursor, pure and noble metal-doped WO_3 nanoplates were synthesized at room temperature by a simple acidification method. It is expected that such combined process will provide a new insight into preparing WO_3 functional nanomaterials by using a cheaper scheelite concentrate as the tungsten source as well as improving sensing properties by utilizing the noble metal element existed in this mineral materials. The in-situ doping of noble metal elements onto WO_3 sensing materials was performed to simulate their existence in tungsten raw material, and their effects on microstructure and NO_2 sensing performance of the products were also investigated systemically.

2. Experimental

2.1. Materials

In this work, a low-grade scheelite concentrate was used as the tungsten source, which was purchased from Gansu Xinzhou Mining Co., Ltd. And all chemical reagents (Kemiou Chemical Reagent Co., Ltd) used for the present work were of analytical grade without any subsequent purification treatment. Deionized water was

directly used in all experimental operations.

The X-ray Fluorescence spectrometry (XRF) and X-ray diffraction (XRD) were performed to determine the chemical compositions of the low-grade scheelite concentrate before the experiments, and the corresponding results are illustrated in Table 1 and Fig. 1, respectively. It can be observed from Table 1 that the main valuable composition of the scheelite concentrate sample is WO_3 , and the main impurity components are SiO_2 , CaO , P_2O_5 , Fe_2O_3 , MgO and SO_3 . It can be seen from Fig. 1 that tungsten in the scheelite concentrate exists in the form of CaWO_4 .

2.2. Synthesis of WO_3 nanoplates

The synthesis of pure, Ag-, Pd-, Au-, and Pt-doped WO_3 nanoplates mainly includes the following three steps.

Firstly, the scheelite concentrate was converted into water-soluble Na_2WO_4 compound by leaching experiments. All the leaching experiments were performed in a microform high-pressure autoclave with a volume of 250 mL. The apparatus equipped with a stirring speed controller and a temperature controller was purchased from Shanghai Yanzhen Co., Ltd. In the preparation process, 5 g of scheelite concentrate, 3.51 g of sodium hydroxide, and 5 mL of deionized water were added into the above autoclave. Then, the leaching experiments were performed for 120 min at the reaction temperature of 180°C with a stirring speed of 400 rpm. After naturally cooling down to 50°C , the digested slurry was removed and then treated by washing and filtering to obtain the sodium tungstate-containing leaching solution. The main chemical compositions of the as-obtained leaching solution were analyzed by inductively

coupled plasma atomic emission spectrometry (ICP-AES), and the corresponding results are shown in Table 2. The obtained leaching solution mainly contains W and trace of impurities such as Si and Mo. The content of other impurities in the leaching solution are close to those in tungsten-containing chemical purity or analytical purity, which have no effect on the later preparation of WO_3 nanomaterials.

Secondly, the sodium tungstate in leaching solution was converted to calcium tungstate by a simple chemical precipitation. 5 mL of the above leaching solution was added into a 250 mL beaker and then 70 mL of deionized water was added to dilute the leaching solution. The pH value of the diluted leaching solution was above 13. Subsequently, to obtain Ag-, Pd-, Au-, and Pt-doped WO_3 nanoplates, a certain amount of silver nitrate solution (1.699 g/L), palladium chloride solution (1.773 g/L), chloroauric acid solution (5.850 g/L) or chloroplatinic acid solution (6.706 g/L) was added into the above diluted leaching solution to ensure the molar ratio of Ag/W, Pd/W, Au/W or Pt/W to be 0.7 mol%, and the as-obtained homogeneous solution was determined as solution A. 2 g of CaCl_2 was added into 20 mL of deionized water and continuously stirred to form solution B. Subsequently, the solution B was slowly added into the solution A and vigorously stirred for 10 min. In the case, a large amount of white precipitate, namely calcium tungstate, was formed. The obtained white precipitate was separated by washing and filtering by using deionized water, and subsequently dried in a drying oven.

Thirdly, WO_3 nanoplates doped with Ag, Pd, Au and Pt were prepared at room temperature by a simple acidification method. The dried white product was added into

20 mL of 4 M HNO₃ and continuously stirred for 24 h. Then, the as-obtained products were washed and filtered by using deionized water, and subsequently dried in a drying oven for 12 h. To obtain more stable WO₃ nanoplates, the dried products were annealed for 4 h at 400 °C in a tube furnace.

2.3. Structural characterizations

The elemental components of the scheelite concentrate were determined by X-ray Fluorescence spectrometry (XRF, Shimadzu XRF-1800). The crystalline structure and phase purity of the scheelite concentrate and the as-synthesized WO₃ nanoplates were analyzed by X-ray diffraction (XRD, PANalytical X'Pert Pro) with K α radiation and copper target in diffraction angle ranges of 10–90° and 15–70°, respectively. The main elemental compositions of the leaching solution were examined by inductively coupled plasma atomic emission spectrometry (ICP-AES, Thermo Fisher Scientific). The surface morphology and microstructure of the WO₃ samples were characterized by using a field-emission scanning electron microscope (FESEM, ZEISS Ultra Plus) and a high-resolution transmission electron microscope (TEM, FEIG²-20) equipped with an energy-dispersive spectroscopy (EDS). The elemental components and elemental valence of the WO₃ products were examined by X-ray photoelectron spectroscopy (XPS, ESCALAB 250 Xi) using Al K α radiation. The main chemical groups of the as-synthesized WO₃ nanoplates were analyzed by Fourier transform infrared spectroscopy (FTIR, NICOLET 380). The specific surface areas of the as-obtained WO₃ samples were analyzed by a Brunauer-Emmet-Teller (BET, Micro-meritics ASAP 2020 instruments, USA) method.

2.4. Fabrication of gas sensor device

The WO₃ nanoplates-based gas sensor devices were prepared as below: firstly, a moderate amount of the as-synthesized WO₃ nanomaterial and absolute ethanol were put into 1.5 mL centrifugal tube and then ultrasonically dispersed for 15 min to form a viscous paste. Secondly, the paste was uniformly coated on the outer surface of an Al₂O₃ ceramic tube equipped with four Pt lead wires and two Au electrodes to form the sensing film. As a resistance heater, a Ni-Cr alloy heating coil was inserted through the ceramic tube to control the desired operating temperature. Subsequently, the WO₃ nanoplates-coated Al₂O₃ ceramic tube was directly welded to a pedestal with six probes to assemble the final sensor device. Finally, to enhance the long-term stability and repeatability of the WO₃ nanoplates, all sensor devices were aged in ambient air at 300 °C for 24 h before use.

2.5. Gas sensing measurements

Gas sensing measurements of pure, Ag-, Pd-, Au-, and Pt-doped WO₃ nanoplates were performed in a fume hood with a relative humidity (RH) of below 30% by using a static gas-sensing system (WS-30A, Weisheng Electronics Co., Ltd). The operating temperature (T_{op}) of the WO₃ sensor was adjusted from 75 to 225 °C by changing the heating voltage. In order to obtain the fixed NO₂ concentration in the range of 50 ppb–5 ppm, a certain volume of NO₂ with the original concentration of 0.02% was injected into the test chamber with a capacity of 18 L by a syringe. The resistance value of the as-prepared WO₃ nanoplates-based sensor was determined by monitoring the voltage signal, where 5 V dc bias was used between two Au electrodes. The

responses (S) of the sensor exposed to reducing and oxidizing gases were calculated based on the equations of R_a/R_g and R_g/R_a , respectively, where R_g and R_a referred to the sensor resistance in the presence and absence of detected gas, respectively [37]. The response time (T_{res}) was defined as the time for the sensor to reach 90% of the whole resistance change in the case of the chemisorption of NO_2 molecules, and the recovery time (T_{rec}) was the required time for the sensor to fall to 10% of its base resistance in the case of the desorption of NO_2 molecules [38].

3. Results and discussion

3.1. Structural and morphological characteristics

The EDS analysis of pure WO_3 nanoplates was firstly carried out to determine whether there were other impurities in the WO_3 sample, and the result is illustrated in Fig. 2(a). It demonstrates that the WO_3 products consist of two elements of W and O, demonstrating that the products show high purity. Fig. 2(b) further investigates the phase purity and crystal structure of pure and noble metal-doped WO_3 samples by XRD. As observed in Fig. 2(b), the peaks of all the as-synthesized WO_3 samples can be matched well with monoclinic-structured WO_3 , which are in good agreement with the standard data file (JCPDS No. 43-1035). The peaks of (200), (020), and (002) planes are all narrow and strong, indicating that all the as-prepared WO_3 products have good crystallinity. Obviously, the main peaks of pure and noble metal-doped WO_3 samples have the same position in the XRD patterns. Additionally, the

diffraction peaks corresponding to other components are not observed, further revealing that no other impurities are observed in the WO_3 products prepared from a low-grade scheelite concentrate. More importantly, no diffraction peaks related to Ag, Pd and Pt elements are found, which may be ascribed to the low content of noble metal in the WO_3 products. A small reflection peak correlated to (111) from Au (JCPDS No. 04-0784) can be found, which indicates the existence of Au in WO_3 .

Fig. 3 illustrates the low- and high-magnification SEM images of pure and noble metal-doped WO_3 nanoplates. It can be clearly seen from the low-magnification SEM images (Fig. 3a, 3d, 3j and 3m) that compared with other WO_3 samples, the Au-doped WO_3 nanoplates sample (Fig. 3j) has the worst dispersibility. As seen from the high-magnification SEM images, all the WO_3 products are composed of interlaced and irregular nanoplates with the thickness of 10–30 nm, and the length and width of the nanoplates are in the range of several hundred nanometers. These WO_3 nanoplates in different directions loosely stack together and correspondingly create a large number of porous passageways, which is helpful to the diffusion of gaseous molecules and the subsequent interaction between gaseous molecules and sensing material.

TEM and HRTEM were also employed to further determine the microstructure and crystallinity of the as-prepared WO_3 nanoplates, and the corresponding results are presented in Fig. 4. As clearly seen from the TEM images (Fig. 4a, 4c, 4e and 4g), except for many nanoplates, there are some black rod-shaped shadows in the field of view. These shadows are the nanoplates perpendicular to the plane, which further

confirms the hierarchical nanoplate structure of the as-prepared WO_3 samples. Such results are in good accordance with the SEM observation, which is helpful to improve gas sensing properties due to its porosity structure. The clear lattice fringes can be seen from HRTEM images, revealing the high crystallinity of these WO_3 nanomaterials. The inter-planar spacings of 0.364 nm (Fig. 4b, 4d and 4f) and 0.384 nm (Fig. 4h) can match well with the (200) and (002) planes of monoclinic-structured WO_3 , respectively, which are in accordance with the XRD results. The interplanar spacings of 0.243 and 0.181 nm in Fig. 4b can be in good accordance with the (111) plane of Ag and the (102) plane of Ag_2O , respectively, demonstrating the existence of Ag in the form of silver metal (Ag^0) and silver oxide (Ag_2O). The inter-planar spacings of 0.215 nm in Fig. 4(d), 0.204 nm in Fig. 4(f), and 0.226 nm in Fig. 4(h) can match well with the (111) plane of PdO_2 , the (200) plane of Au, and the (111) plane of PtO_2 , respectively, indicating that these noble metal elements exist in the form of metallic or metallic oxide nanoparticles. The SAED pattern inserted in each TEM image further reveals that the noble metal-doped WO_3 nanoplates belong to polycrystalline structure.

The elemental mapping images were investigated to further verify the existence and distribution state of noble metal elements in the WO_3 samples and the corresponding results are illustrated in Fig. 5. As observed in this figure, each WO_3 sample consists of W, O, and corresponding noble metal element. More importantly, for each WO_3 sample, the noble metal elements are uniformly distributed in the visible area.

The surface chemical components and electronic structures of noble metal-doped WO_3 nanoplates measured by XPS are illustrated in Fig. 6. The binding energies of all the WO_3 samples were calibrated with reference to the C 1s peak (284.8 eV). As seen in Fig. 6(a), the W 4f spectra of noble metal-doped WO_3 nanoplates have two strong peaks centered at 35.68–35.88 eV and 37.88–37.98 eV, which can be identified to the binding energies of W 4f_{7/2} and W 4f_{5/2}, respectively, demonstrating that the tungsten in the WO_3 crystal exists as W^{6+} [25, 39]. As observed in Fig. 6(b), the peaks of noble metal-doped WO_3 nanoplates centered at 530.38–530.58 eV are corresponding to O 1s, which can be contributed to lattice oxygen (O^{2-}) in WO_3 lattice [8, 40]. Fig. 6(c) displays that the doublets located at 368.38 and 374.28 eV are attributed to Ag 3d_{5/2} and Ag 3d_{3/2}, respectively, of which one is related to a single silver metal (Ag^0) and the other is in accordance with a silver oxide (Ag_2O) due to the partial surface oxidization of Ag [15, 41]. Fig. 6(d) shows that the peak situated at 338.11 eV is contributed to Pd 3d of a palladium oxide (PdO_2) [42, 43]. Fig. 6(e) presents that two strong peaks situated at 83.99 and 87.68 eV, respectively, which correspond to Au 4f_{7/2} and Au 4f_{5/2}, implying the existence of Au nanoparticles in the Au-doped WO_3 crystals [44]. Fig. 6(f) shows that the peak located at 79.26 eV is ascribed to Pt 4f, indicating that Pt exists in the WO_3 sample in the form of PtO_2 [45].

Fig. 7 illustrates the FTIR spectra of pure and noble metal-doped WO_3 nanoplates in the wavenumber range of 500–4000 cm^{-1} . It can be clearly observed that there are some differences in these FTIR spectra. For all the WO_3 samples, the peak positions are basically same, but the intensities of the peaks related to some special

functional groups change slightly. Meanwhile, for each WO_3 sample, no peaks correlated to corresponding noble metal element are found because of the low content of noble metal in the WO_3 nanoplates. Furthermore, there are no other peaks related to some impurity components, demonstrating that all the WO_3 samples are of high purity. The peaks situated at $\sim 3425 \text{ cm}^{-1}$ are corresponding to $-\text{OH}$ stretching vibration [25]. The peaks positioned at $\sim 1631 \text{ cm}^{-1}$ are contributed to O-H bending vibration band. The peaks at $\sim 968 \text{ cm}^{-1}$ are assigned to $\text{W}=\text{O}$ bond stretching. The peaks at $\sim 732 \text{ cm}^{-1}$ are attributed to the W-O-W stretching vibration of the bridging oxygen [25].

Fig. 8 illustrates the N_2 adsorption-desorption isotherms of pure and noble metal-doped WO_3 samples. All the WO_3 samples exhibit type-IV isotherms with H3 hysteresis loops, indicating that the WO_3 samples have typical mesoporous structure. The average specific surface areas of the pure, Ag-, Pd-, Au-, and Pt-doped WO_3 samples are determined to be 27.57, 34.93, 36.38, 42.84 and 42.31 m^2/g , respectively. It can be concluded that the specific surface area of pure WO_3 nanoplates is greatly improved by noble metal doping, which is conducive to enhancing the sensing properties of the samples.

3.2. Gas sensing properties

The responses of pure and noble metal-doped WO_3 nanoplates to 5 ppm NO_2 at 75–225 °C are illustrated in Fig. 9(a). As is well-known, the sensor response mainly depends on the operating temperature due to its influence on the thermodynamics and kinetics of the chemisorption of gaseous molecules on the surface active sites of the

sensing materials. For all sensors, there are similar change trends, i.e., the responses of all WO_3 nanoplates to 5 ppm NO_2 increase gradually and then reach a maximal value along with increasing the operating temperature. As a result, an optimal operating temperature of 175 °C for pure and Au-doped WO_3 nanoplates, and 150 °C for Ag-, Pd- and Pt-doped WO_3 nanoplates are respectively achieved to balance the activation and desorption of gas molecules, thereby obtaining a peak response for each sensor [37]. Obviously, the responses of noble metal-doped WO_3 nanoplates are significantly higher than those of pure WO_3 nanoplates. Especially, the Pd-doped WO_3 nanoplates exhibit highest response value at a relatively low operating temperature of 150 °C. Compared with pure and Au-doped WO_3 nanoplates, Ag-, Pd-, and Pt-doped WO_3 nanoplates obviously reduce the optimal operating temperature at which the peak response can be obtained. The above results can be contributed to the different catalytic activities of the noble metal nanoparticles as well as the varied work function energies of WO_3 and noble metal elements.

Fig. 9(b) presents the base resistance values of pure and noble metal-doped WO_3 nanoplates at 75–225 °C in air. Obviously, all the base resistance values of noble metal-doped WO_3 nanoplates are higher than those of pure WO_3 nanoplates due to the different work function energies of WO_3 and noble metal elements, resulting in the formation of Schottky junctions in the contact interfaces of WO_3 and noble metal. It should be mentioned that the base resistance value of Au-doped WO_3 nanoplates at 75 °C is not presented here because its base resistance is too large to be detected at a relatively low operating temperature. When the operating temperature is below 100 °C,

the base resistance values of all the as-synthesized WO_3 sensing materials are higher than $100 \text{ M}\Omega$. However, the values rapidly decrease as the operating temperature further increases. Especially, the values obtained at the optimal operating temperature of $150 \text{ }^\circ\text{C}$ for Ag-, Pd- and Pt-doped WO_3 nanoplates or $175 \text{ }^\circ\text{C}$ for pure and Au-doped WO_3 nanoplates are less than $100 \text{ M}\Omega$, revealing that all the as-prepared WO_3 sensing materials can meet the requirement of the practical application. As observed from the inserted image, the base resistance value has a good linear relationship with the operating temperature in the range of $125\text{--}175 \text{ }^\circ\text{C}$. Therefore, the base resistances at $125\text{--}175 \text{ }^\circ\text{C}$ are chosen to calculate the activation energies of the reactions between the as-synthesized WO_3 sensing materials and NO_2 molecules. The activation energies are calculated according to the Arrhenius' equation of $\ln(1/R)=A-E/KT$, where R is resistance, A is Arrhenius constant, T is Kelvin temperature, K is Boltzmann constant, and E is energy barrier [32]. The calculated results are illustrated in Fig. 9(c). According to the calculated results, the activation energies of the reactions between pure, Ag-, Pd-, Au-, and Pt-doped WO_3 nanoplates and NO_2 are 0.84, 0.22, 0.20, 0.58 and 0.68 eV, respectively. Correspondingly, the response values to 5 ppm NO_2 at $150 \text{ }^\circ\text{C}$ are obviously improved in the following order: pure, Pt-, Au-, Ag-, and Pd-doped WO_3 nanoplates. This further proves that the sensor response has a direct relationship with the activation energy of the reaction between sensing material and NO_2 . Noble metal doping can obviously reduce the activation energy of the reaction between sensing material and NO_2 , which is helpful to the chemical adsorption of oxygen species and the acceleration of the surface

chemical reactions of the sensing materials, and the subsequently enhancement of NO₂ sensing performance. In addition, the larger specific surface area can also be beneficial to the enhancement of the sensor response.

Fig. 9(d) shows the dynamic response curves of pure and noble metal-doped WO₃ nanoplates to 5 ppm NO₂ at their optimal operating temperatures. For each sensor, the response quickly increases along with the injection of NO₂ into test chamber, and then decreases along with the release of NO₂, implying that the WO₃ nanoplates are classified to n-type metal oxide semiconductor material. Meanwhile, it also shows that the sensor responses at their optimal operating temperatures are obviously improved in the order as follows: pure, Pt-, Ag-, Au-, and Pd-doped WO₃ nanoplates, demonstrating that the catalytic effect of Pd is obviously stronger in comparison with those of other noble metals and the catalytic effect of Pt is relatively weaker in this case.

Fig. 9(e-f) illustrates the response times and recovery times of pure and noble metal-doped WO₃ nanoplates to 5 ppm NO₂ at 75–225 °C. It can be seen in Fig. 9(e) that the response speed of noble metal-doped WO₃ nanoplates is significantly faster than that of pure WO₃ nanoplates at a fixed operating temperature, indicating that noble metal doping can effectively accelerate the chemisorption of detected gaseous molecules on the surface active sites and subsequently promote their chemical reactions with sensing materials. This is mainly attributed to the catalytic activity of noble metal nanoparticles and the low activation energies of the reactions between sensing materials and NO₂. However, the changes in the recovery time of noble

metal-doped WO_3 nanoplates are relatively complex. It can be clearly observed in Fig. 9(f) that the recovery times of noble metal-doped WO_3 nanoplates are usually longer than those of pure one below $125\text{ }^\circ\text{C}$, and the corresponding values are shorter than those of pure one above $175\text{ }^\circ\text{C}$. It should be mentioned that the recovery time of pure WO_3 nanoplates at $75\text{ }^\circ\text{C}$ is not illustrated in Fig. 9(f) because it takes a long time to recover to its initial value at such low operating temperature.

Fig. 10(a-b) illustrates the dynamic response curves of the WO_3 nanoplates-based sensors towards 50 ppb, 100 ppb, 300 ppb, 500 ppb, 1 ppm, 3 ppm and 5 ppm NO_2 at their optimal operating temperatures. For each sensor, the amplitude change in the sensor response increases as NO_2 concentration increases. For a fixed NO_2 concentration, the increase in the response follows the injection of NO_2 , and subsequently decreases after the release of NO_2 from the test chamber, indicating a good reversibility. Additionally, the lowest detection concentration is 50 ppb, indicating that the as-obtained WO_3 nanoplates can be used for the detection of ppb-level NO_2 .

The corresponding responses of pure and noble metal-doped WO_3 nanoplates to various concentrations of NO_2 at their optimal operating temperatures are illustrated in Fig. 10(c-d). For each sensor, the response increases as NO_2 concentration increases, demonstrating that the sensor does not reach the saturation state for the adsorption of NO_2 molecules. This may be attributed to the large effective specific surface area of the WO_3 nanoplates, which can supply more surface sites for the chemisorption reactions of gas molecules.

The correspondingly enlarged response images of pure and noble metal-doped WO₃ nanoplates-based sensors in the NO₂ concentration range of 1–5 ppm at their optimal operating temperatures are shown in Fig. 10(e). The linear correlation coefficients (R^2) of the sensor response curves as a function of NO₂ concentration are above 0.90, indicating a good linearly relationship with NO₂ concentration for each sensor. The slopes calculated based on the above curves of pure, Ag-, Pd-, Au- and Pt-doped WO₃ nanoplates are 8.11, 30.61, 51.77, 25.83 and 9.32, respectively. Therefore, Pd-doped WO₃ nanoplates can supply more surface active sites for the chemisorption of NO₂ molecules along with further increasing NO₂ concentration and exhibit highest response in comparison with other sensors, which further proves that the lower activation energy induced by the catalytic effect of noble metal is helpful to the enhancement of the sensor response.

The relationship between sensor response and NO₂ concentration can be estimated by the theory of power laws: $S=k[C_{NO_2}]^m+1$, where C_{NO_2} refers to NO₂ concentration, S is sensor response, m is an exponent, and k is a constant. The calculated results are illustrated in Fig. 10(f). As seen in this figure, the sensor response linearly increases as NO₂ concentration increases from 50 ppb to 5 ppm for each sensor, which can be used to assess NO₂ concentration based on its sensor response value.

A summary presented in Fig. 11 is made to further determine the effect of noble metal element on NO₂ sensing properties of the WO₃ nanoplates in terms of response, response/recovery time as well as operating temperature. Some important results are

summarized as below. (1) Compared with Au doping, the doping of Ag, Pd and Pt can effectively reduce optimal operating temperature. (2) Noble metal doping can obviously improve the sensor response, especially Pd doping. (3) Noble metal doping can significantly reduce response time, especially Ag-doped WO_3 nanoplates-based sensor shows the shortest response time. (4) Compared with response time, the recovery time changes relatively complex after noble metal doping, and Pd doping obviously reduces the recovery time, while Ag doping increases the recovery time. Although Au doping cannot reduce the optimal operating temperature, the peak response is still higher, and the response/recovery time is relatively shorter. Pt doping can reduce the optimal operating temperature, but the enhancement of NO_2 sensing properties is not obvious. The above results are mainly ascribed to the synergistic effect of the large specific surface area, the sensitization effects of noble metal nanoparticles and the varied work function energies of WO_3 and noble metal elements together with the different activation energies of the reactions between sensing materials and NO_2 . The detail sensing mechanism will be discussed later.

To further estimate NO_2 sensing performance of the as-synthesized WO_3 nanomaterials, some comparisons between the as-prepared WO_3 nanoplates and other nanostructured WO_3 materials were conducted in terms of operating temperature, response, response/recovery time as well as detection limit. The results are illustrated in Table 3. Obviously, these WO_3 sensors in previous reports still have more or less drawbacks, such as low response, slow response/recovery speed and high operating temperature, which restrict their practical applications. Although the Ag-, Pd-, Au-,

and Pt-doped WO_3 nanoplates are synthesized from a low-grade scheelite concentrate, the WO_3 nanoplates-based sensors show excellent NO_2 sensing performance compared with other WO_3 sensors reported in the literatures. Additionally, such sensors can be used to detect low-concentration NO_2 , and the detection limit is even as low as 50 ppb.

Fig. 12(a-b) presents the reproductive cycles of pure and noble metal-doped WO_3 nanoplates-based sensors exposed to 5 ppm NO_2 at their optimal operating temperatures. The results show that the amplitude change in the sensor response is basically same at a fixed concentration of NO_2 . It suggests good repeatability and excellent stability of the present WO_3 nanomaterials, which is beneficial to their practical application. Fig. 12(c) illustrates the long-term stability of the WO_3 nanoplates-based sensors to 5 ppm NO_2 at their optimal operating temperatures. As seen in this figure, all the sensors exhibit a good stability during the test cycle of 30 days. Fig. 12(d) presents the selectivity of pure and noble metal-doped WO_3 nanoplates-based sensors towards various kinds of toxic gases, including NO_2 , methanol, NH_3 , acetone, methylbenzene, methanal, and SO_2 at their optimal operating temperatures. Obviously, all the sensors exhibit extraordinary selectivity towards NO_2 in comparison with other detected gases. The prominent NO_2 selectivity can be attributed to the chemical reactions on the surfaces of WO_3 sensing materials between NO_2 molecules and chemisorbed oxygen species.

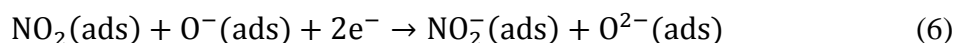
3.3. Gas sensing mechanism

As a typical n-type metal oxide semiconductor, WO_3 belongs to

surface-controlled type of the sensing material. Hence, the change in the sensor resistance is relevant to the chemisorption of detected gaseous molecules as well as the chemical reactions between these gaseous molecules and chemical components on the WO_3 surface [48]. The commonly accepted sensing mechanism of the WO_3 nanomaterial is the surface-depletion model [49]. The schematic illustration of NO_2 sensing mechanism of noble metal-doped WO_3 nanoplates is presented in Fig. 13.

The enhanced NO_2 sensing properties of noble metal-doped WO_3 nanoplates can be ascribed to the large specific surface area of WO_3 nanoplates, the sensitization effects of noble metal nanoparticles, and the varied work function energies of metal noble and WO_3 together with the different activation energies of the reactions between WO_3 sensing materials and NO_2 . The work function energies of WO_3 and noble metals [3, 5, 50-54], and the activation energies of the reactions between the WO_3 sensing materials and NO_2 are listed in Table 4. As seen from Table 4, noble metal doping can significantly reduce the activation energy of the reaction between WO_3 sensing material and NO_2 induced by the catalytic effect of noble metal, which is helpful to the improvement of gas sensing properties. It can also be seen from the table that the work function energy of each noble metal is different from that of WO_3 , resulting in the formation of Schottky junctions in the contact interfaces of noble metal and WO_3 . Subsequently, the electrons transfer is accelerated, leading to a broadening in the width of interfacial electron depletion layer. Correspondingly, the WO_3 sensing materials are more sensitive to the detected gas molecules. According to the results illustrated in Fig. 10(b), the base resistance values in air of noble

metal-doped WO₃ nanoplates are higher than those of pure WO₃ nanoplates at 75–225 °C, demonstrating that the width of electron depletion layer increases after doping noble metals [55]. As actively catalytic components, noble metal nanoparticles in WO₃ nanoplates can accelerate the diffusion of oxygen molecules onto the surface sites and extract free electrons from the WO₃ conduction band by the conversion of gas molecules and ions, which improves the quality and quantity of the chemical adsorbed oxygen ions (O²⁻, O₂⁻ and O⁻) and simultaneously generates more surface effective adsorption sites [34, 56]. These effective adsorption sites are beneficial to the fast diffusion of NO₂ molecules and the subsequent ionization of NO₂ to NO₂⁻ (NO₂+e⁻→NO₂⁻) on the WO₃ surface. Because the optimal operating temperature for pure and noble metal-doped WO₃ nanoplates is between 100 to 300 °C, the oxygen species on the surface of WO₃ mainly exist as O⁻. Thus, the chemical reaction relative to the above can be presented as follows [17, 25].



Meanwhile, the noble metal nanoparticles on the WO₃ surface will create more adsorption sites to adsorb and catalytically dissociate oxygen molecules, which are conducive to improving the sensitivity [57]. Compared with other noble metal-doped

WO₃ nanoplates, the Pd-doped WO₃ nanoplates exhibit a highest response to NO₂ and a shortest recovery time at 150 °C due to the smallest activation energy, indicating that the catalytic effect of Pd is relatively stronger in comparison with those of other noble metals. The Pt-doped WO₃ nanoplates show a relatively lower response to NO₂, and a longer response/recovery time because of the relatively higher activation energy, indicating that the catalytic effect of Pt are relatively lower.

4. Conclusions

The interlaced and irregular WO₃ nanoplates with a single monoclinic structure were synthesized from a low-grade scheelite concentrate by three combined processes including NaOH leaching, chemical precipitation, and acidification. Meanwhile, the in-situ doping of noble metal elements into WO₃ nanoplates was carried out to simulate their existence in tungsten raw material and their effects on microstructure and NO₂ sensing properties were also investigated. The microstructure characterization demonstrated that the thickness of all WO₃ nanoplates was 10–30 nm, and the length and width of these nanoplates were several hundred nanometers. The noble metal nanoparticles were uniformly distributed in the corresponding noble metal-doped WO₃ sample. NO₂ sensing properties indicated that noble metal doping could effectively enhance the sensor response to NO₂ as well as reduce response time. Especially, the doping of Ag, Pd and Pt could obviously reduce optimal operating temperature. Different behaviors in the improvement of NO₂ sensing properties could

be explained by the specific surface area of WO_3 nanoplates, the catalytic activities of noble metal elements, the work function energies of WO_3 and noble metal as well as the activation energies of the reactions between sensing materials and NO_2 . In addition, this work provides a new idea to prepare functional WO_3 sensing nanomaterials by using a low-grade scheelite concentrate as the tungsten source as well as improving gas sensing properties by simulating the existence of noble metal elements in tungsten raw materials. The noble metal-doped WO_3 nanoplates synthesized from a low-grade scheelite concentrate exhibited obviously enhanced NO_2 sensing properties, which have a potential application in environmental detection.

Acknowledgement

The project was supported by the National Natural Science Foundation of China (51674067, 51422402), Fundamental Research Funds for the Central Universities (N180102032, N180106002, N180408018, N170106005), Liaoning Revitalization Talents Program (XLYC1807160), Liaoning BaiQianWan Talents Program (201892127), and Open Foundation of State Key Laboratory of Mineral Processing (BGRIMM-KJSKL-2019-12).

References

- [1] C. Kamble, M. Panse, IDE embedded tungsten trioxide gas sensor for sensitive NO₂ detection, *Mater. Chem. Phys.* 224 (2019) 257-263.
- [2] L. Yang, A. Marikutsa, M. Rummyantseva, E. Konstantinova, N. Khmelevsky, A. Gaskov, Quasi similar routes of NO₂ and NO sensing by nanocrystalline WO₃: Evidence by in situ DRIFT spectroscopy, *Sensors* 19 (2019) 3405.
- [3] Y. Shen, H. Bi, T. Li, X. Zhong, X. Chen, A. Fan, D. Wei, Low-temperature and highly enhanced NO₂ sensing performance of Au-functionalized WO₃ microspheres with a hierarchical nanostructure, *Appl. Surf. Sci.* 434 (2018) 922-931.
- [4] M.S. Choi, H.G. Na, A. Mirzaei, J.H. Bang, W. Oum, S. Han, S.-W. Choi, M. Kim, C. Jin, S.S. Kim, H.W. Kim, Room-temperature NO₂ sensor based on electrochemically etched porous silicon, *J. Alloys Compd.* 811 (2019) 151975.
- [5] P. Jaroenapibal, P. Boonma, N. Saksilaporn, M. Horprathum, V. Amornkitbamrung, N. Triroj, Improved NO₂ sensing performance of electrospun WO₃ nanofibers with silver doping, *Sens. Actuators B* 255 (2018) 1831-1840.
- [6] J. Sun, J. Guo, J. Ye, B. Song, K. Zhang, S. Bai, R. Luo, D. Li, A. Chen, Synthesis of Sb doping hierarchical WO₃ microspheres and mechanism of enhancing sensing properties to NO₂, *J. Alloys Compd.* 692 (2017) 876-884.
- [7] H. Zhang, Y. Wang, X. Zhu, Y. Li, W. Cai, Bilayer Au nanoparticle-decorated WO₃ porous thin films: On-chip fabrication and enhanced NO₂ gas sensing performances with high selectivity, *Sens. Actuators B* 280 (2019) 192-200.

- [8] B. Behera, S. Chandra, Synthesis of WO_3 nanorods by thermal oxidation technique for NO_2 gas sensing application, *Mater. Sci. Semicond. Process* 86 (2018) 79-84.
- [9] Z. Zhang, M. Haq, Z. Wen, Z. Ye, L. Zhu, Ultrasensitive ppb-level NO_2 gas sensor based on WO_3 hollow nanosphers doped with Fe, *Appl. Surf. Sci.* 434 (2018) 891-897.
- [10] Jyoti, G.D. Varma, Enhanced room temperature sensitivity of Ag-CuO nanobrick/reduced graphene oxide composite for NO_2 , *J. Alloys Compd.* 806 (2019) 1469-1480.
- [11] X. Chen, Y. Shen, P. Zhou, S. Zhao, X. Zhong, T. Li, C. Han, D. Wei, D. Meng, NO_2 sensing properties of one-pot-synthesized ZnO nanowires with Pd functionalization, *Sens. Actuators B* 280 (2019) 151-161.
- [12] K.K. Pawar, J.S. Shaikh, S.S. Mali, Y.H. Navale, V.B. Patil, C.K. Hong, P.S. Patil, Hollow In_2O_3 microcubes for sensitive and selective detection of NO_2 gas, *J. Alloys Compd.* 806 (2019) 726-736.
- [13] Y. Shen, X. Zhong, J. Zhang, T. Li, S. Zhao, B. Cui, D. Wei, Y. Zhang, K. Wei, In-situ growth of mesoporous In_2O_3 nanorod arrays on a porous ceramic substrate for ppb-level NO_2 detection at room temperature, *Appl. Surf. Sci.* 498 (2019) 143873.
- [14] Y. Shen, B. Zhang, X. Cao, D. Wei, J. Ma, L. Jia, S. Gao, B. Cui, Y. Jin, Microstructure and enhanced H_2S sensing properties of Pt-loaded WO_3 thin films, *Sens. Actuators B* 193 (2014) 273-279.
- [15] Y. Wang, X. Cui, Q. Yang, J. Liu, Y. Gao, P. Sun, G. Lu, Preparation of Ag-loaded

- mesoporous WO_3 and its enhanced NO_2 sensing performance, *Sens. Actuators B* 225 (2016) 544-552.
- [16] X. Zhong, Y. Shen, S. Zhao, X. Chen, C. Han, D. Wei, P. Fang, D. Meng, SO_2 sensing properties of SnO_2 nanowires grown on a novel diatomite-based porous substrate, *Ceram. Int.* 45 (2019) 2556-2565.
- [17] X. Chen, Y. Shen, X. Zhong, T. Li, S. Zhao, P. Zhou, C. Han, D. Wei, Y. Shen, Synthesis of ZnO nanowires/ Au nanoparticles hybrid by a facile one-pot method and their enhanced NO_2 sensing properties, *J. Alloys Compd.* 783 (2019) 503-512.
- [18] X. San, G. Wang, B. Liang, J. Ma, D. Meng, Y. Shen, Flower-like NiO hierarchical microspheres self-assembled with nanosheets: Surfactant-free solvothermal synthesis and their gas sensing properties, *J. Alloys Compd.* 636 (2015) 357-362.
- [19] P. Zhou, Y. Shen, S. Zhao, G. Li, Y. Yin, R. Lu, S. Gao, C. Han, D. Wei, NO_2 sensing properties of WO_3 porous films with honeycomb structure, *J. Alloys Compd.* 789 (2019) 129-138.
- [20] T. Li, Y. Shen, S. Zhao, X. Chen, G. Li, R. Lu, L. Zhu, H. Li, D. Wei, Xanthate sensing properties of Pt-functionalized WO_3 microspheres synthesized by one-pot hydrothermal method, *Ceram. Int.* 44 (2018) 4814-4823.
- [21] A. Marikutsa, L. Yang, M. Romyantseva, M. Batuk, J. Hadermann, A. Gaskov, Sensitivity of nanocrystalline tungsten oxide to CO and ammonia gas determined by surface catalysts, *Sens. Actuators B* 277 (2018) 336-46.
- [22] C.C. Jia, X. Zhang, K. Matras-Postolek, B.B. Huang, P. Yang, Z-scheme reduced graphene oxide/ TiO_2 -Bronze/ $\text{W}_{18}\text{O}_{49}$ ternary heterostructure towards efficient full

- solar-spectrum photocatalysis, *Carbon* 139 (2018) 415-26.
- [23] B. Miao, W. Zeng, Y. Mu, W. Yu, S. Hussain, S. Xu, H. Zhang, T. Li, Controlled synthesis of monodisperse $\text{WO}_3 \cdot \text{H}_2\text{O}$ square nanoplates and their gas sensing properties, *Appl. Surf. Sci.* 349 (2015) 380-386.
- [24] F. Li, Q. Qin, N. Zhang, C. Chen, L. Sun, X. Liu, Y. Chen, C. Li, S. Ruan, Improved gas sensing performance with Pd-doped $\text{WO}_3 \cdot \text{H}_2\text{O}$ nanomaterials for the detection of xylene, *Sens. Actuators B* 244 (2017) 837-848.
- [25] T. Li, Y. Shen, S. Zhao, X. Zhong, W. Zhang, C. Han, D. Wei, D. Meng, Y. Ao, Sub-ppm level NO_2 sensing properties of polyethyleneimine-mediated WO_3 nanoparticles synthesized by a one-pot hydrothermal method, *J. Alloys Compd.* 783 (2019) 103-112.
- [26] C. Song, C. Li, Y. Yin, J. Xiao, X. Zhang, M. Song, W. Dong, Preparation and gas sensing properties of partially broken WO_3 nanotubes, *Vacuum* 114 (2015) 13-16.
- [27] Y. Yu, W. Zeng, M. Xu, X. Peng, Hydrothermal synthesis of $\text{WO}_3 \cdot \text{H}_2\text{O}$ with different nanostructures from 0D to 3D and their gas sensing properties, *Physica E* 79 (2016) 127-132.
- [28] S. Cao, C. Zhao, T. Han, L. Peng, Hydrothermal synthesis, characterization and gas sensing properties of the WO_3 nanofibers, *Mater. Lett.* 169 (2016) 17-20.
- [29] S. Zhao, Y. Shen, P. Zhou, X. Zhong, C. Han, Q. Zhao, D. Wei, Design of $\text{Au}@\text{WO}_3$ core-shell structured nanospheres for ppb-level NO_2 sensing, *Sens. Actuators B* 282 (2019) 917-922.
- [30] Y.-S. Shim, L. Zhang, D.H. Kim, Y.H. Kim, Y.R. Choi, S.H. Nahm, C.-Y. Kang, W.

- Lee, H.W. Jang, Highly sensitive and selective H₂ and NO₂ gas sensors based on surface-decorated WO₃ nanoigloos, *Sens. Actuators B* 198 (2014) 294-301.
- [31] F. Gu, Y. Cui, D. Han, S. Hong, M. Flytzani-Stephanopoulos, Z. Wang, Atomically dispersed Pt (II) on WO₃ for highly selective sensing and catalytic oxidation of triethylamine, *Appl. Catal. B-Environ.* 256 (2019) 117809.
- [32] A. Koo, R. Yoo, S.P. Woo, H.-S. Lee, W. Lee, Enhanced acetone-sensing properties of Pt-decorated Al-doped ZnO nanoparticles, *Sens. Actuators B* 280 (2019) 109-119.
- [33] C. Feng, Z. Jiang, J. Wu, B. Chen, G. Lu, C. Huang, Pt-Cr₂O₃-WO₃ composite nanofibers as gas sensors for ultra-high sensitive and selective xylene detection, *Sens. Actuators B* 300 (2019) 127008.
- [34] J.M. Walker, S.A. Akbar, P.A. Morris, Synergistic effects in gas sensing semiconducting oxide nano-heterostructures: A review, *Sens. Actuators B* 286 (2019) 624-40.
- [35] C. Kamble, M. Panse, A. Nimbalkar, Ag decorated WO₃ sensor for the detection of sub-ppm level NO₂ concentration in air, *Mater. Sci. Semicond. Processing* 103(2019) 104613.
- [36] C.-H. Wu, Z. Zhu, S.-Y. Huang, R.-J. Wu, Preparation of palladium-doped mesoporous WO₃ for hydrogen gas sensors, *J. Alloys Compd.* 776(2019) 965-73.
- [37] F. Li, S. Guo, J. Shen, L. Shen, D. Sun, B. Wang, Y. Chen, S. Ruan, Xylene gas sensor based on Au-loaded WO₃·H₂O nanocubes with enhanced sensing performance, *Sens. Actuators B* 238 (2017) 364-373.

- [38] M. He, L. Xie, X. Zhao, X. Hu, S. Li, Z.-G. Zhu, Highly sensitive and selective H₂S gas sensors based on flower-like WO₃/CuO composites operating at low/room temperature, *J. Alloys Compd.* 788 (2019) 36-43.
- [39] M. Yin, Y. Yao, H. Fan, S. Liu, WO₃-SnO₂ nanosheet composites: Hydrothermal synthesis and gas sensing mechanism, *J. Alloys Compd.* 736 (2018) 322-331.
- [40] Y. Zhu, H. Wang, J. Liu, M. Yin, L. Yu, J. Zhou, Y. Liu, F. Qiao, High-performance gas sensors based on the WO₃-SnO₂ nanosphere composites, *J. Alloys Compd.* 782 (2019) 789-795.
- [41] Z. Wang, Y. Zhang, S. Liu, T. Zhang, Preparation of Ag nanoparticles-SnO₂ nanoparticles-reduced graphene oxide hybrids and their application for detection of NO₂ at room temperature, *Sens. Actuators B* 222 (2016) 893-903.
- [42] K. Dhara, K. Sarkar, D. Srimani, S.K. Saha, P. Chattopadhyay, A. Bhaumik, A new functionalized mesoporous matrix supported Pd (II)-Schiff base complex: an efficient catalyst for the Suzuki–Miyaura coupling reaction, *Dalton Trans.* 39 (2010) 6395-402.
- [43] V. Alegre, M. Da Silva, M. Schmal, Catalytic combustion of methane over palladium alumina modified by niobia, *Catal. Commun.* 7 (2006) 314-22.
- [44] S. Kabcum, N. Kotchasak, D. Channei, A. Tuantranont, A. Wisitsoraat, S. Phanichphant, C. Liewhiran, Highly sensitive and selective NO₂ sensor based on Au-impregnated WO₃ nanorods, *Sens. Actuators B* 252 (2017) 523-536.
- [45] C.K. Acharya, W. Li, Z. Liu, G. Kwon, C. Heath Turner, A.M. Lane, D. Nikles, T. Klein, M. Weaver, Effect of boron doping in the carbon support on platinum

- nanoparticles and carbon corrosion, *J. Power Sources* 192 (2009) 324-9.
- [46] M. Penza, C. Martucci, G. Cassano, NO_x gas sensing characteristics of WO₃ thin films activated by noble metals (Pd, Pt, Au) layers, *Sens. Actuators B* 50 (1998) 52-59.
- [47] H. Xia, Y. Wang, F. Kong, S. Wang, B. Zhu, X. Guo, J. Zhang, Y. Wang, S. Wu, Au-doped WO₃-based sensor for NO₂ detection at low operating temperature, *Sens. Actuators B* 134 (2008) 133-9.
- [48] Y. Wang, C. Liu, Z. Wang, Z. Song, X. Zhou, N. Han, Y. Chen, Sputtered SnO₂:NiO thin films on self-assembled Au nanoparticle arrays for MEMS compatible NO₂ gas sensors, *Sens. Actuators B* 278 (2019) 28-38.
- [49] S. An, S. Park, H. Ko, C. Lee, Fabrication of WO₃ nanotube sensors and their gas sensing properties, *Ceram. Int.* 40 (2014) 1423-1429.
- [50] Z. Wang, S. Huang, G. Men, D. Han, F. Gu, Sensitization of Pd loading for remarkably enhanced hydrogen sensing performance of 3DOM WO₃, *Sens. Actuators B* 262 (2018) 577-87.
- [51] D. Yamashita, A. Ishizaki, In situ measurements of change in work function of Pt, Pd and Au surfaces during desorption of oxygen by using photoemission yield spectrometer in air, *Appl. Surf. Sci.* 363 (2016) 240-4.
- [52] X. Buwen, S. Yafeng, M. Meng, L. Chuannan, Enhancement of hole injection with an ultra-thin Ag₂O modified anode in organic light-emitting diodes, *Microelectron. J.* 36 (2005) 105-8.
- [53] S. Aggarwal, A. Monga, S. Perusse, R. Ramesh, V. Ballarotto, E. Williams, B.

- Chalamala, Y. Wei, R. Reuss, Spontaneous ordering of oxide nanostructures, Science 287 (2000) 2235-7.
- [54] A. Staerz, Y. Liu, U. Geyik, H. Brinkmann, U. Weimar, T. Zhang, N. Barsan, The effect of platinum loading on WO₃ based sensors, Sens. Actuators B 291 (2019) 378-84.
- [55] T.H. Kim, A. Hasani, L.V. Quyet, Y. Kim, S.Y. Park, M.G. Lee, W. Sohn, T.P. Nguyen, K.S. Choi, S.Y. Kim, H.W. Jang, NO₂ sensing properties of porous Au-incorporated tungsten oxide thin films prepared by solution process, Sens. Actuators B 286 (2019) 512-520.
- [56] Y. Mun, S. Park, S. An, C. Lee, H.W. Kim, NO₂ gas sensing properties of Au-functionalized porous ZnO nanosheets enhanced by UV irradiation, Ceram. Int. 39 (2013) 8615-8622.
- [57] P. Van Tong, N.D. Hoa, N. Van Duy, D.T.T. Le, N. Van Hieu, Enhancement of gas-sensing characteristics of hydrothermally synthesized WO₃ nanorods by surface decoration with Pd nanoparticles, Sens. Actuators B 223 (2016) 453-460.

Figure captions

Fig. 1. XRD pattern of the scheelite concentrate.

Fig. 2. (a) EDS spectrum of pure WO₃ nanoplates. (b) XRD patterns of pure and noble metal-doped WO₃ nanoplates.

Fig. 3. Low- and high-magnification SEM images of pure and noble metal-doped WO₃ nanoplates. (a-c) Pure WO₃. (d-f) Ag-doped WO₃. (g-i) Pd-doped WO₃. (j-l) Au-doped WO₃. (m-o) Pt-doped WO₃.

Fig. 4. TEM and HRTEM images of noble metal-doped WO₃ nanoplates. (a-b) Ag-doped WO₃. (c-d) Pd-doped WO₃. (e-f) Au-doped WO₃. (g-h) Pt-doped WO₃. The insert in each TEM image presents the corresponding SAED pattern.

Fig. 5. Elemental mapping images of noble metal-doped WO₃ nanoplates. (a-d) Ag-doped WO₃. (e-h) Pd-doped WO₃. (i-l) Au-doped WO₃. (m-p) Pt-doped WO₃.

Fig. 6. XPS spectra of noble metal-doped WO₃ nanoplates. (a) W 4f peaks. (b) O 1s peaks. (c) Ag 3d peaks. (d) Pd 3d peak. (e) Au 4f peaks. (f) Pt 4f peak.

Fig. 7. FTIR spectra of pure and noble metal-doped WO₃ nanoplates.

Fig. 8. N₂ adsorption-desorption isotherms of pure and noble metal-doped WO₃ samples.

Fig. 9. (a) Response curves and (b) base resistance values in air of WO₃ nanoplates to 5 ppm NO₂ at 75–225 °C. (c) Corresponding Arrhenius plots at 125–175 °C. (d) Dynamic response curves of WO₃ nanoplates to 5 ppm NO₂ at their optimal operating temperatures. (e) Response times and (f) recovery times of WO₃ nanoplates to 5 ppm NO₂ at 75–225 °C.

Fig. 10. (a-b) Dynamic response curves of the sensors based on WO₃ nanoplates as a function of NO₂ concentration ranging from 50 ppb to 5 ppm at their optimal operating temperatures. (c-d) The corresponding response values at different concentrations of NO₂. (e) Enlarged response images in the NO₂ concentration range of 1–5 ppm at their optimal operating temperatures. (f) Plots of $\ln(S-1)$ vs. $\ln[C_{NO_2}]$ for WO₃ nanoplates at their optimal operating temperatures.

Fig. 11. Summary of NO₂ sensing properties of pure and noble metal-doped WO₃ nanoplates at a fixed NO₂ concentration of 5 ppm. (a) The optimal operating temperature. (b) The peak responses at their optimal operating temperatures. (c) Response time and (d) recovery time at 150 °C.

Fig. 12. (a-b) Reproductive cycles and (c) long-term stability of the sensors based on

WO₃ nanoplates towards 5 ppm NO₂ at their optimal operating temperatures. (d) Comparisons of the sensor responses to various kinds of detected gases at their optimal operating temperatures.

Fig. 13. Schematic illustration of the adsorption reaction of NO₂ molecules on the surfaces of (a) pure and (b) noble metal-doped WO₃ nanoplates, and (c) the energy band change of noble metal-doped WO₃ nanoplates before and after the adsorption of NO₂ molecules.

Table 1 Main chemical compositions of the scheelite concentrate.

Table 2 Main chemical compositions of the leaching solution.

Table 3 Comparison of NO₂ sensing properties of noble metal-doped WO₃ nanoplates-based sensors with other sensors.

Table 4 Work function energies of WO₃ and noble metals, and the activation energies of the reactions between the WO₃ sensing materials and NO₂.

Table 1 Main chemical compositions of the scheelite concentrate.

Element	WO ₃	CaO	SiO ₂	P ₂ O ₅	MgO	SO ₃
Content / wt. %	62.36	19.11	5.55	3.99	2.82	2.17
Element	Fe ₂ O ₃	F	Al ₂ O ₃	MoO ₃	As ₂ O ₃	BaO
Content / wt. %	1.55	0.69	0.60	0.25	0.02	0.35

Table 2 Main chemical compositions of the leaching solution.

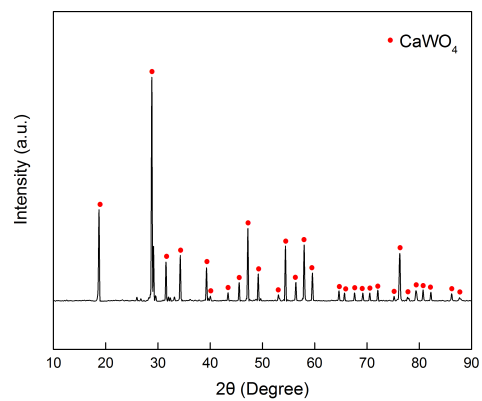
Element	W	Si	Mo	As
Content g/L	122.2	0.33	0.52	0.061

Table 3 Comparison of NO₂ sensing properties of noble metal-doped WO₃ nanoplates-based sensors with other sensors.

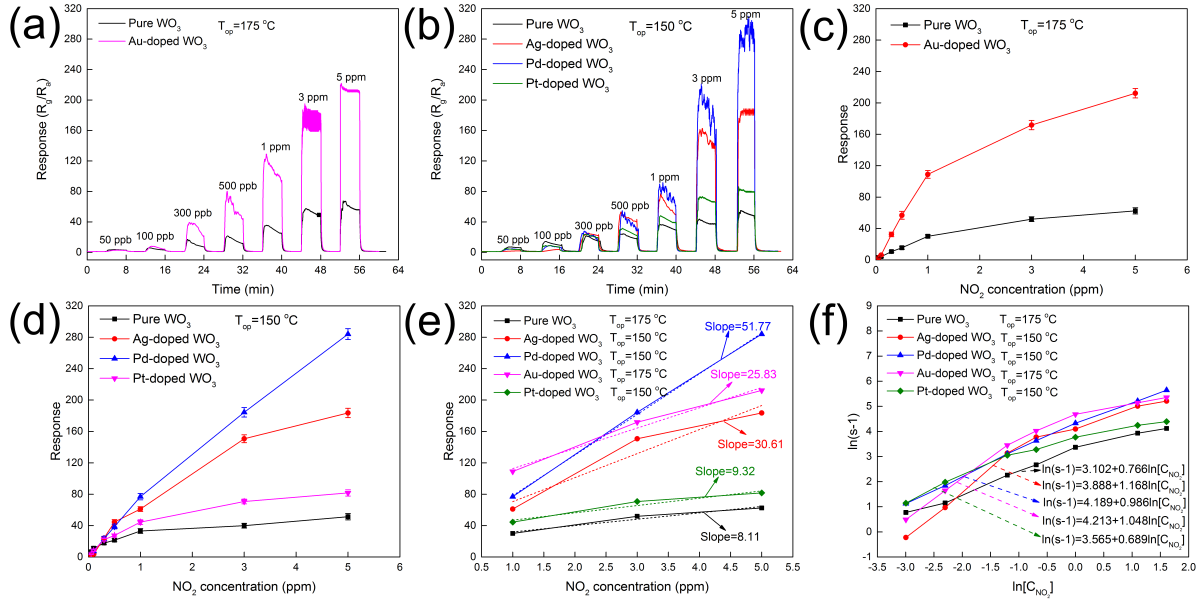
Material	T_{op} (°C)	NO₂ (ppm)	Response	T_{res}/T_{rec} (s)	Detection limit (ppm)	Reference
Ag-doped WO ₃ nanofibers	225	5	90.3	714/522	0.5	[5]
WO ₃ thin film activated by Pd layer	200	10	6.51	162/240	1	[46]
Ag-functionalized WO ₃ nanoigloos	200	3	12.22	41/97	0.1	[35]
Au-doped WO ₃ nanoparticles	150	5	100	~	5	[47]
Ag-WO ₃ film	200	3	12.22	41/97	0.1	[35]
Au-impregnated WO ₃ nanorods	250	5	836.6	64.2/~	0.125	[44]
WO ₃ thin film activated by Pt layer	150	10	3.45	210/360	1	[46]
Ag-doped WO ₃ nanoplates	150	5	183.54	14/189	0.05	Present work
Pd-doped WO ₃ nanoplates	150	5	283.96	26/66	0.05	Present work
Au-doped WO ₃ nanoplates	175	5	212.29	9/108	0.05	Present work
Pt-doped WO ₃ nanoplates	150	5	81.68	36/131	0.05	Present work

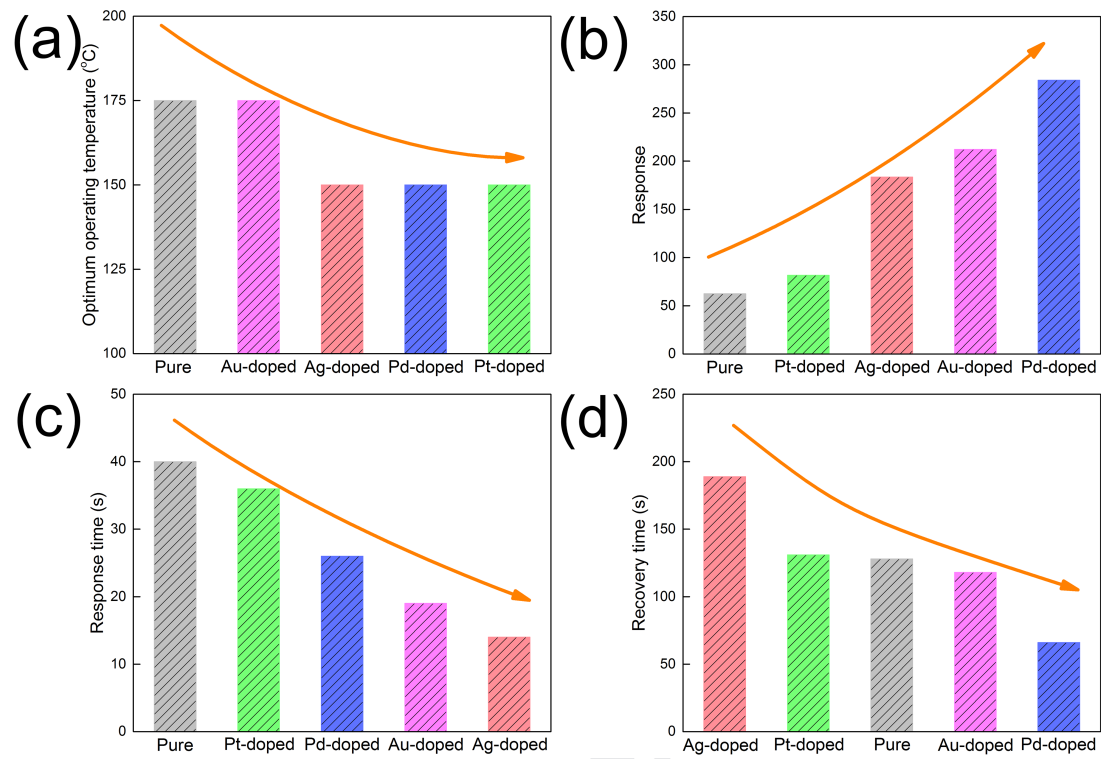
Table 4 Work function energies of WO₃ and noble metals, and the activation energies of the reactions between the WO₃ sensing materials and NO₂.

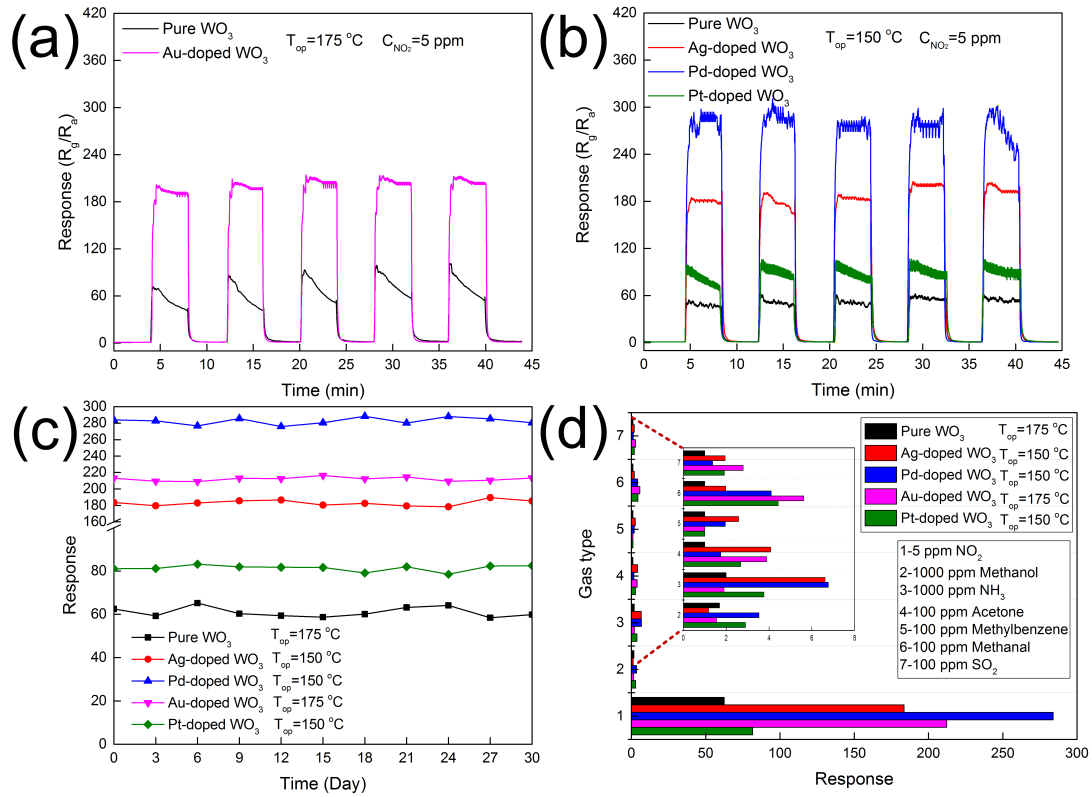
Work function energy / eV	WO ₃	Ag/Ag ₂ O	PdO ₂	Au	PtO ₂
	5.7	4.26/5.0	3.9	5.65	5.93
Activation energy / eV	Pure WO ₃	Ag-WO ₃	Pd-WO ₃	Au-WO ₃	Pt-WO ₃
	0.84	0.22	0.20	0.58	0.68

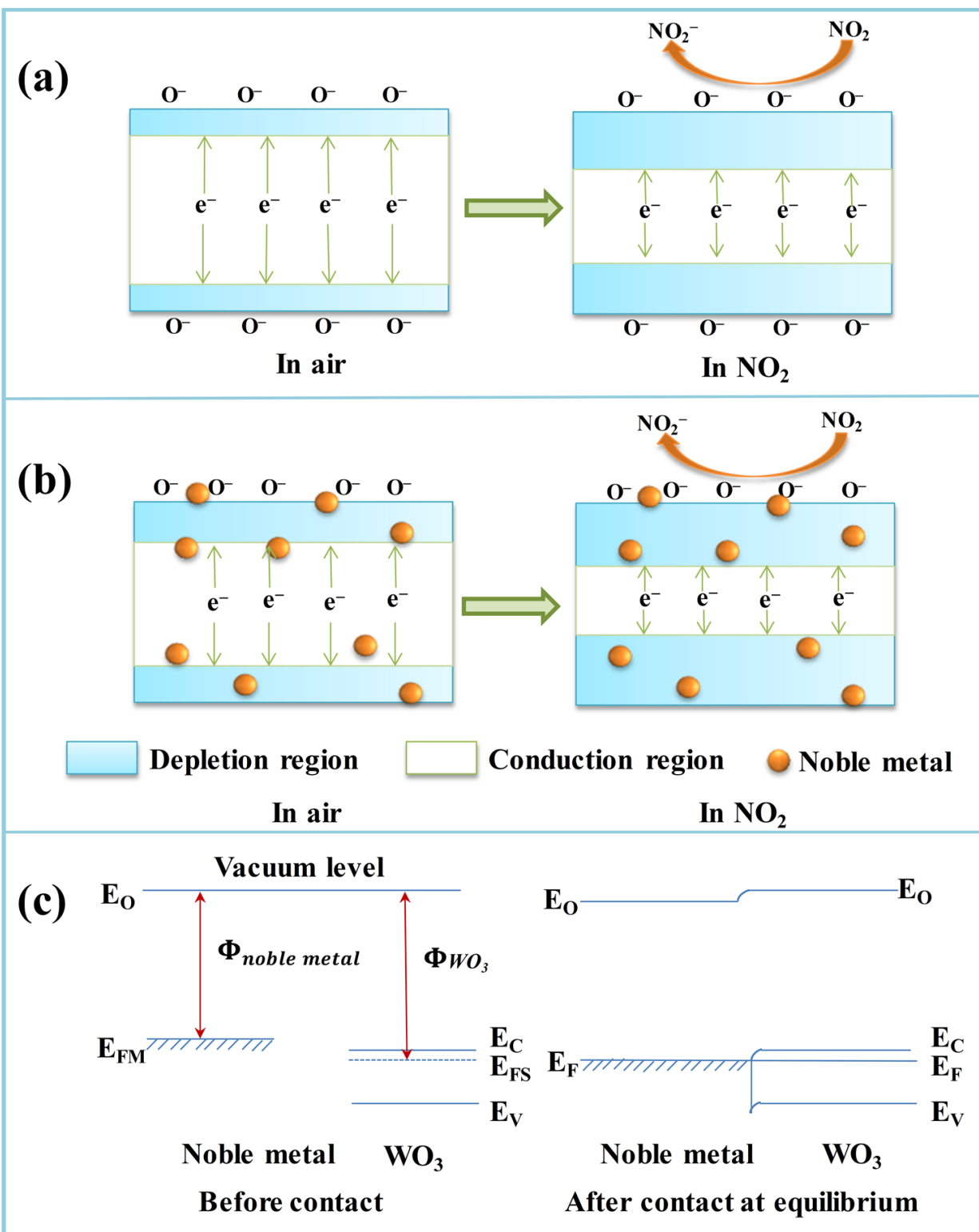


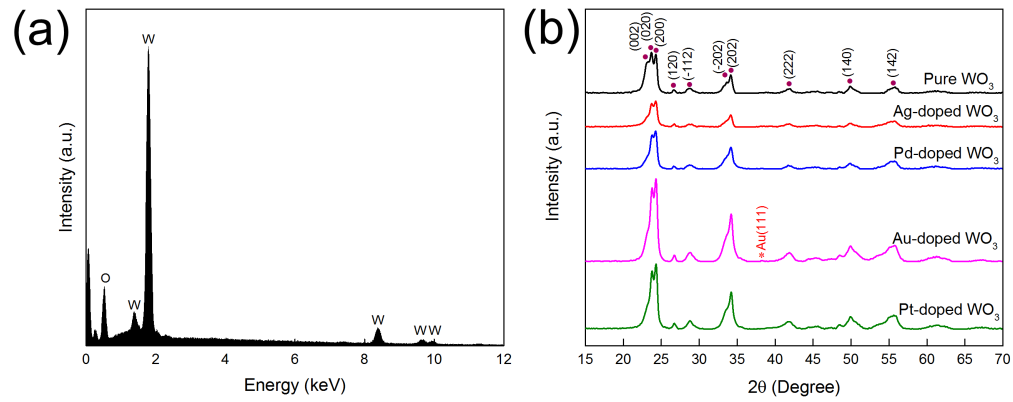
Journal Pre-proof

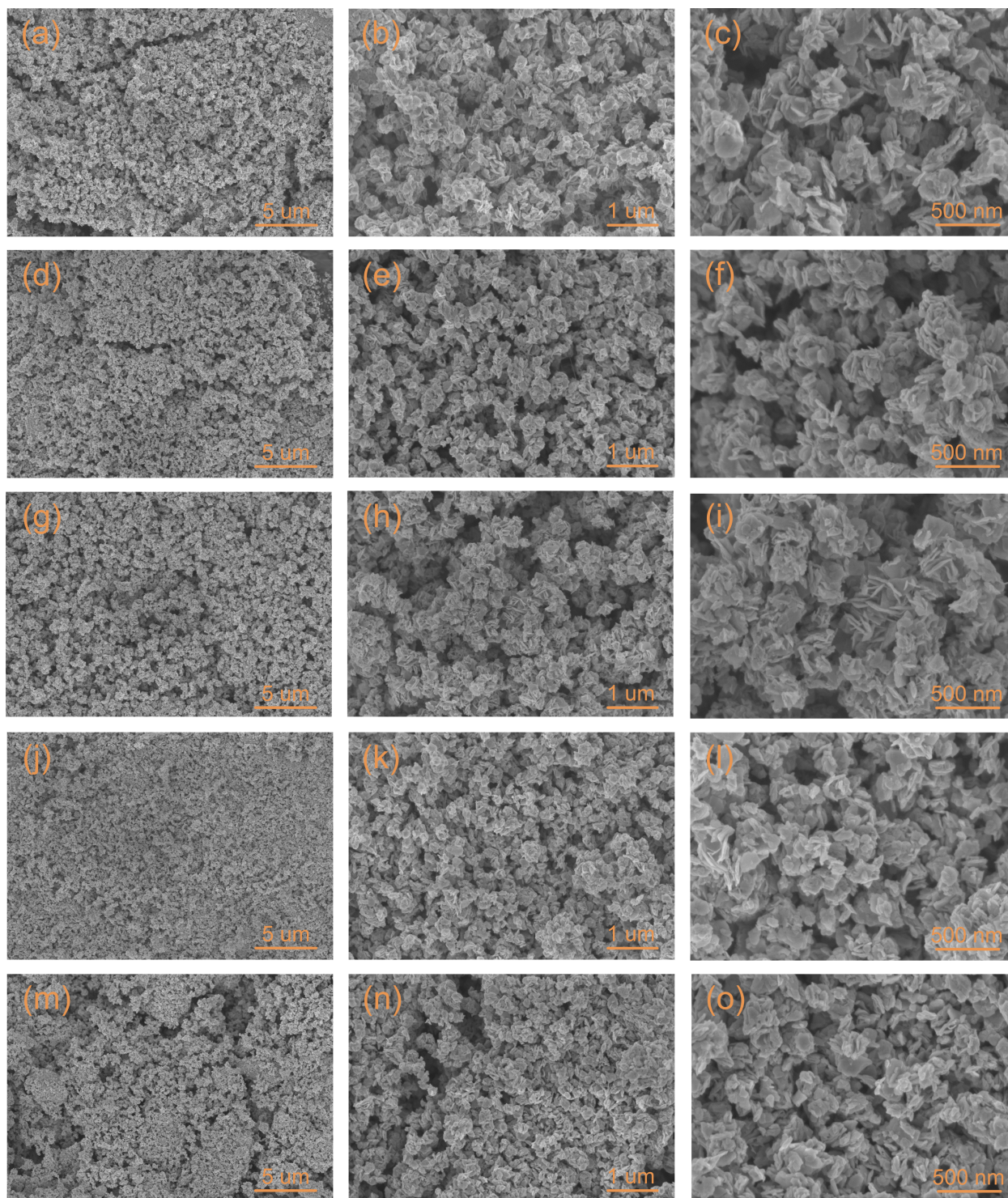


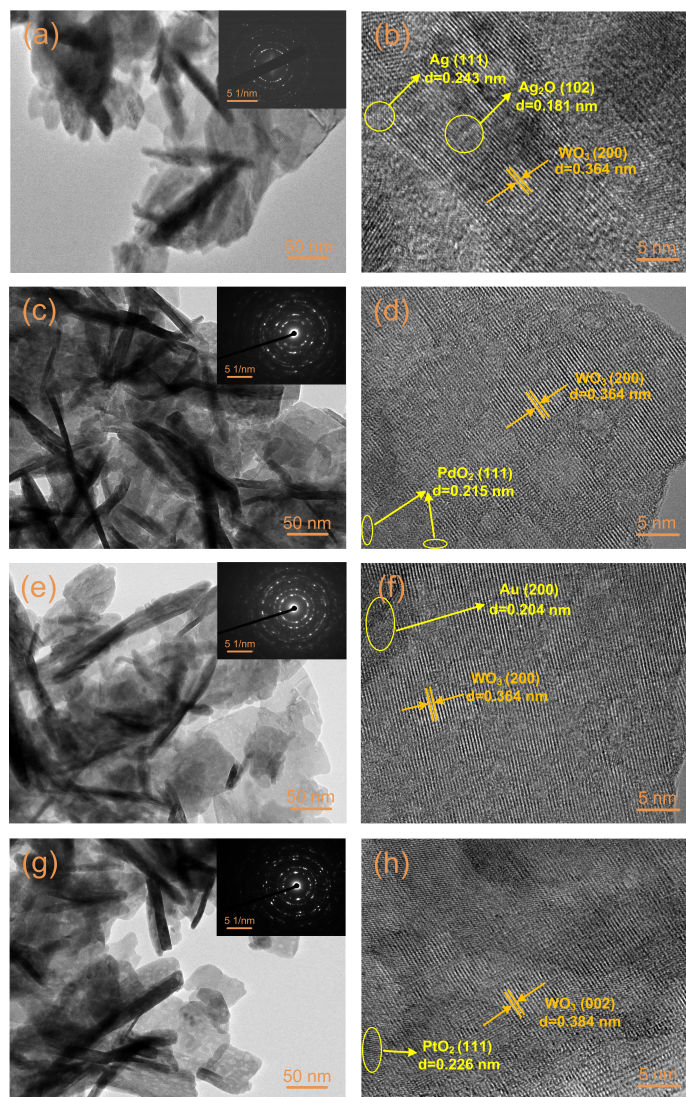


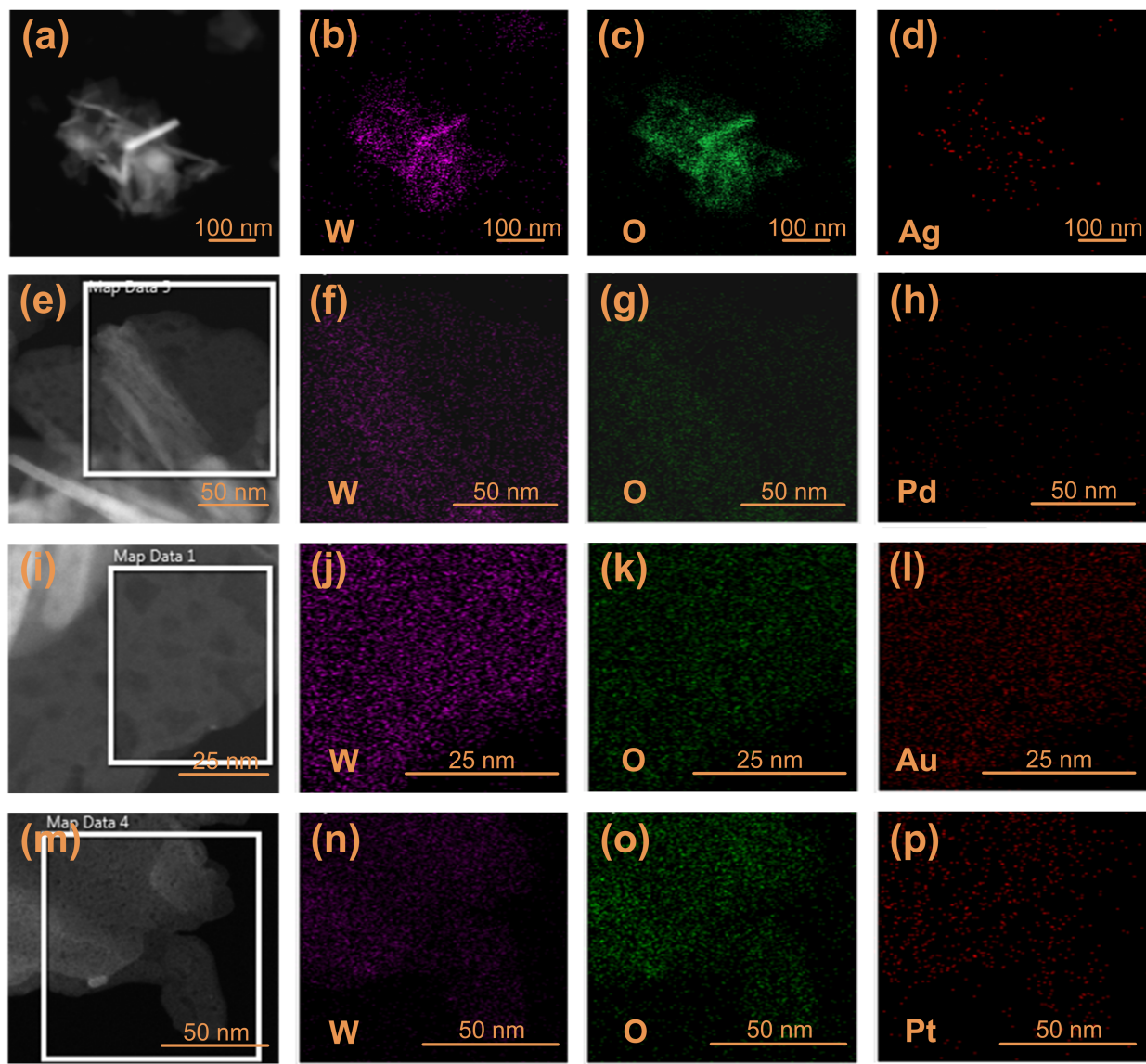


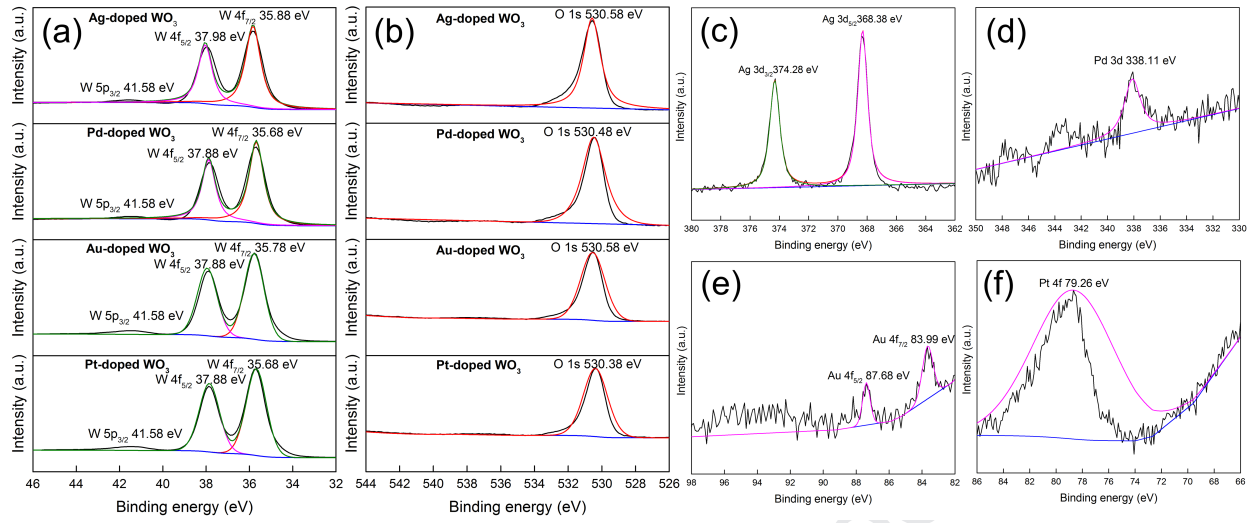


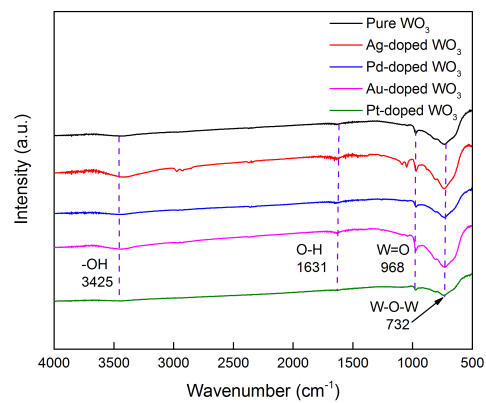




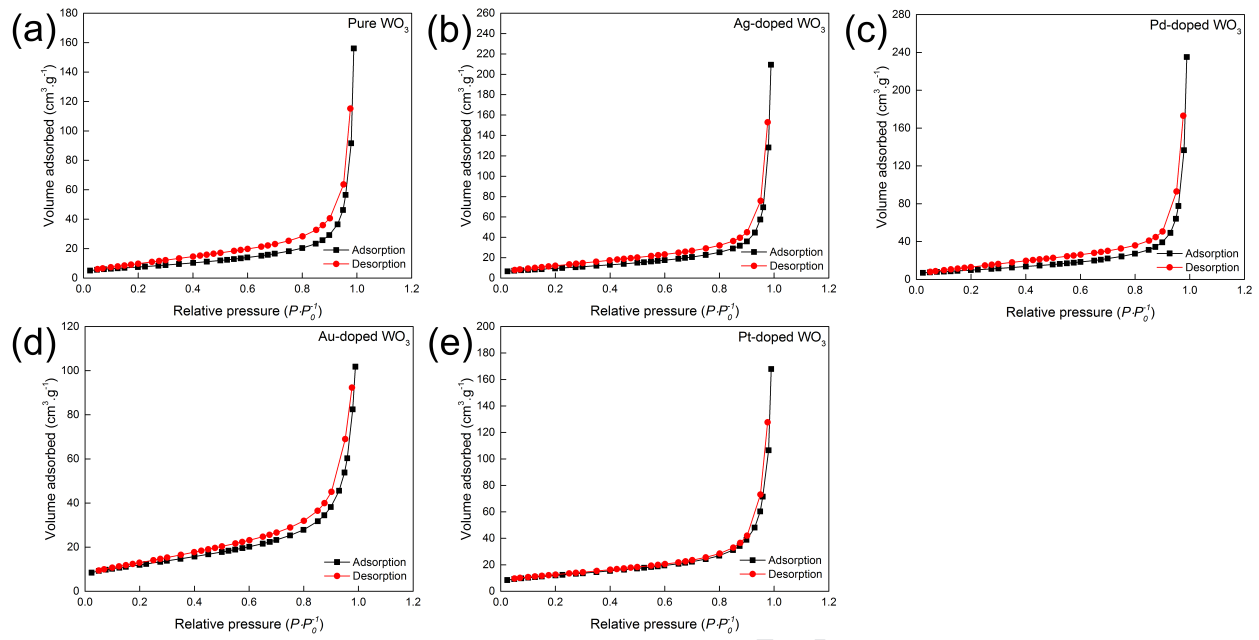


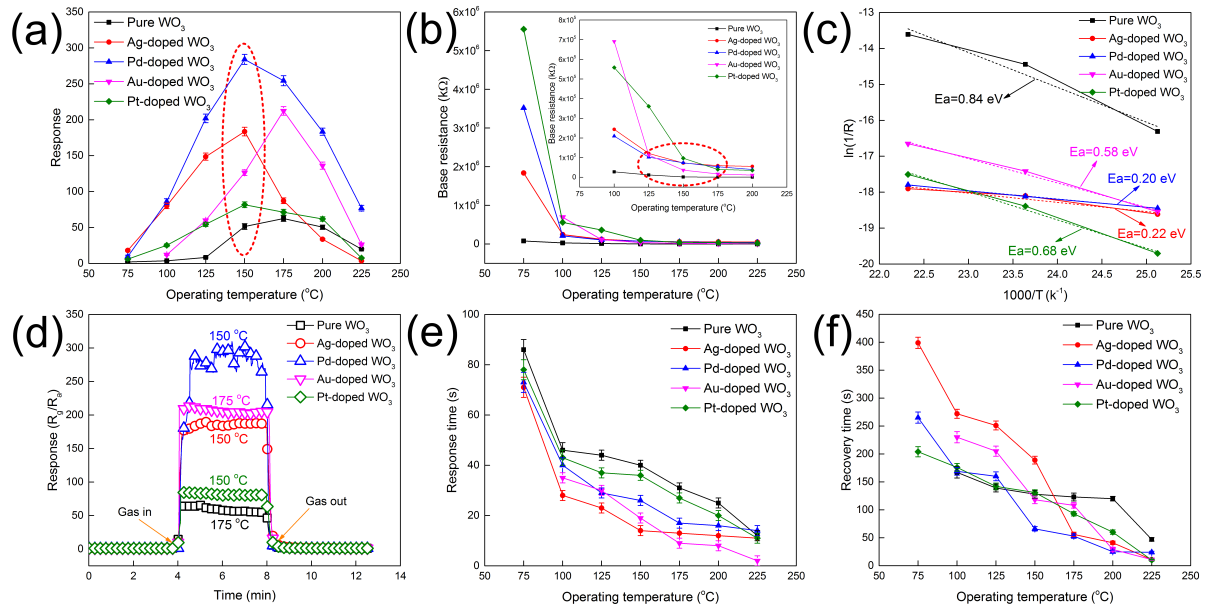






Journal Pre-proof





Highlights

- The monoclinic-structured WO_3 with interlaced and irregular nanoplates were synthesized from a low-grade scheelite concentrate.
- In-situ doping of noble metal elements into WO_3 nanoplates was carried out to simulate their existence in tungsten raw material.
- The noble metal-doped WO_3 nanoplates exhibited distinct behaviors in terms of the enhancement of NO_2 sensing properties.
- The enhanced NO_2 sensing properties of the noble metal-doped WO_3 nanoplates were systematically discussed.

Declaration of interest statement

We declare that we have no financial and personal relationships with other people or organizations that can inappropriately influence our work, there is no professional or other personal interest of any nature or kind in any product, service and/or company that could be construed as influencing the position presented in, or the review of, the manuscript entitled, “Effect of noble metal element on microstructure and NO₂ sensing properties of WO₃ nanoplates prepared from a low-grade scheelite concentrate”.